



This is a repository copy of *Heterogeneous water storage and thermal regime of supraglacial ponds on debris-covered glaciers*.

White Rose Research Online URL for this paper:
<http://eprints.whiterose.ac.uk/121307/>

Version: Accepted Version

Article:

Scott Watson, C., Quincey, D.J. orcid.org/0000-0002-7602-7926, Carrivick, J.L. et al. (3 more authors) (2017) Heterogeneous water storage and thermal regime of supraglacial ponds on debris-covered glaciers. *Earth Surface Processes and Landforms*. ISSN 0197-9337

<https://doi.org/10.1002/esp.4236>

Reuse

Items deposited in White Rose Research Online are protected by copyright, with all rights reserved unless indicated otherwise. They may be downloaded and/or printed for private study, or other acts as permitted by national copyright laws. The publisher or other rights holders may allow further reproduction and re-use of the full text version. This is indicated by the licence information on the White Rose Research Online record for the item.

Takedown

If you consider content in White Rose Research Online to be in breach of UK law, please notify us by emailing eprints@whiterose.ac.uk including the URL of the record and the reason for the withdrawal request.



eprints@whiterose.ac.uk
<https://eprints.whiterose.ac.uk/>

Heterogeneous water storage and thermal regime of supraglacial ponds on debris-covered glaciers

C. Scott Watson¹, Duncan J. Quincey¹, Jonathan L. Carrivick¹, Mark W. Smith¹, Ann V. Rowan², Robert Richardson³

1. School of Geography and water@leeds, University of Leeds, Leeds, UK

2. Department of Geography, University of Sheffield, Sheffield, UK

3. School of Mechanical Engineering, University of Leeds, UK

Correspondence to: C. Scott. Watson (scott@rockyglaciers.co.uk)

Abstract

The water storage and energy transfer roles of supraglacial ponds are poorly constrained, yet they are thought to be important components of debris-covered glacier ablation budgets. We used an unmanned surface vessel (USV) to collect sonar depth measurements for 24 ponds to derive the first empirical relationship between their area and volume applicable to the size distribution of ponds commonly encountered on debris-covered glaciers. Additionally, we instrumented nine ponds with thermistors and three with pressure transducers, characterising their thermal regime and capturing three pond drainage events. The deepest and most irregularly-shaped ponds were those associated with ice cliffs, which were connected to the surface or englacial hydrology network (maximum depth = 45.6 m), whereas hydrologically-isolated ponds without ice cliffs were both more circular and shallower (maximum depth = 9.9 m). The englacial drainage of three ponds had the potential to melt $\sim 100 \pm 20 \times 10^3$ kg to $\sim 470 \pm 90 \times 10^3$ kg of glacier ice owing to the large volumes of stored water. Our observations of seasonal pond growth and drainage with their associated calculations of stored thermal energy have implications for

This article has been accepted for publication and undergone full peer review but has not been through the copyediting, typesetting, pagination and proofreading process which may lead to differences between this version and the Version of Record. Please cite this article as doi: 10.1002/esp.4236

glacier ice flow, the progressive enlargement and sudden collapse of englacial conduits, and the location of glacier ablation hot-spots where ponds and ice cliffs interact. Additionally, the evolutionary trajectory of these ponds controls large proglacial lake formation in deglaciating environments.

Introduction

Debris-covered glaciers are an increasingly common part of the mountain cryosphere, as glacier mass loss promotes the exhumation of englacial rock debris and the development of supraglacial debris layers (Benn et al., 2012; Thakuri et al., 2014). A combination of low glacier surface gradients, stagnating glacier termini and negative mass balance regimes is initiating increased supraglacial water storage on Himalayan debris-covered glaciers through the positive feedback of solar radiation absorption and transmission to glacier ice (Reynolds, 2000; Sakai et al., 2000; Quincey et al., 2007; Benn et al., 2012; Salerno et al., 2012). Coalescing ponds approaching the hydrological base level can ultimately form large proglacial lakes, which are impounded at the edge of a glacier and can expand rapidly through calving (Kirkbride, 1993; Watanabe et al., 1994; Sakai et al., 2009; Rohl, 2008; Carrivick and Tweed, 2013). In this paper we define supraglacial ponds as water bodies $\leq 20,000 \text{ m}^2$ (e.g. Biggs et al., 2005). The expansion of supraglacial ponds and proglacial lakes is ongoing across the central and eastern Himalaya (Komori, 2008; Gardelle et al., 2011; Nie et al., 2013; Wang et al., 2015; Zhang et al., 2015; Watson et al., 2016; Nie et al., 2017), and is of great concern not least due to the potential glacial lake outburst flood (GLOF) hazards for downstream communities and infrastructure (Kattelman, 2003; Benn et al., 2012; Carrivick and Tweed, 2016; Rounce et al., 2016; Rounce et al., 2017a), but also for potential effects on glacier flow dynamics and on glacier mass balance (Carrivick and Tweed, 2013).

Glacial lake bathymetry data are predominantly collected for large proglacial lakes in order to parameterise GLOF hazards or to investigate the ice-marginal lake interactions at glacier calving fronts (Fujita et al., 2009; Shrestha and Nakagawa, 2014; Somos-Valenzuela et al., 2014a; Lamsal et al., 2016; Purdie et al., 2016; Sugiyama et al., 2016). Cook and Quincey (2015) compared three commonly-used empirical relationships between glacial lake area and volume, the latter as derived from some knowledge of lake bathymetry, and replotted a compiled dataset of 75 lake measurements, which included several lakes surveyed multiple times. Their analysis revealed that predicted lake volume can vary by an order of magnitude for a given area due to variable lake bathymetry morphologies. A wide spread of predicted volumes is problematic when attempting to characterise an increasing number of lakes developing in deglaciating basins (Carrivick and Tweed, 2013). Additionally, the bathymetry of proglacial lakes or ponds associated with debris-covered glaciers cannot be derived using remotely sensed imagery due to high turbidity, in contrast to examples of supraglacial lakes from Greenland (e.g. Box and Ski, 2007; Moussavi et al., 2016; Pope et al., 2016). Therefore, there is a clear requirement to better constrain empirical relationships between lake area and volume and to include data from the size distribution of supraglacial ponds typically found on debris-covered glaciers (Cook and Quincey, 2015).

Supraglacial ponds and adjacent ice cliffs appear as hot-spots of melt in multi-temporal digital elevation model (DEM) differencing, in contrast to subdued melt under a thick insulating debris-layer (e.g. Nicholson and Benn, 2013; Immerzeel et al., 2014; Pellicciotti et al., 2015; Ragettli et al., 2016; Thompson et al., 2016). Therefore, quantifying the spatio-temporal dynamics of supraglacial ponds and their interaction with ice cliffs is essential to assess their contribution towards glacier-wide

ablation and seasonal water storage (Miles et al., 2016b; Watson et al., 2016); however, little is known about their seasonal expansion and contraction, thermal regime, or bathymetry. Optical satellite images are often obscured by clouds during the Indian Summer Monsoon, which restricts assessments of seasonal pond dynamics. Cloud-penetrating synthetic aperture radar (SAR) data has been used to map and monitor glacial lake dynamics on the Greenland Ice Sheet (e.g. Miles et al., 2017); however, Himalayan applications are limited to large proglacial lakes thus far (Strozzi et al., 2012). Additionally, studies instrumenting ponds with temperature or water level sensors are rare (e.g. Xin et al., 2012; Horodyskyj, 2015; Miles et al., 2016a; Narama et al., 2017). Notably, the modelling of supraglacial pond energy balance by Sakai et al. (2000) and Miles et al. (2016a) revealed that ponds effectively absorb and transmit thermal energy englacially, and therefore are likely to be key contributors to glacier downwasting.

In this study, we aimed to assess the annual variation in supraglacial pond dynamics and characteristics in order to assess their role for water storage, englacial ablation, and interaction with ice cliffs on debris-covered glaciers. Specifically we: (1) derive the bathymetry, thermal regime, and seasonal water level change, of supraglacial ponds on Khumbu and Lobuche Glaciers in the Everest region of Nepal; (2) use the bathymetry of 24 supraglacial ponds to derive an empirical area-volume relationship; (3) quantify the potential englacial ablation of draining ponds; (4) quantify the variation in pond morphology in relation to the presence of ice cliffs.

Data collection and methods

Study sites

Field data were collected on the debris-covered zones of Khumbu and Lobuche Glaciers in the Everest region of Nepal during three field campaigns (October/November 2015, May 2016, and October 2016) (Figure 1). Khumbu Glacier is ~17 km long with a ~10 km debris-covered ablation area, of which the lower ~4 km is essentially stagnant (Quincey et al., 2009). Within this stagnating part of the glacier, supraglacial ponds are increasingly coalescing to form a connected chain of surface water that is approaching the glacier's hydrological base level (Watson et al., 2016), which is expected to transition into a proglacial lake (Naito et al., 2000; Bolch et al., 2011). By comparison, Lobuche Glacier is smaller, with a relic debris-covered ablation zone ~1 km in length that is now disconnected from clean ice at higher elevations in the accumulation area.

Pond depth surveys

An unmanned surface vessel (USV) was custom-built for the acquisition of global positioning system (GPS)-referenced depth measurements from unfrozen supraglacial ponds (Table 1, Figure 2). The USV was deployed on 24 supraglacial ponds during a field campaign in May 2016 and completed a total survey distance of 18 km. Ponds were surveyed along transects (Figure 2c), although the track spacing was variable between ponds and was greatest for larger ponds.

Supraglacial pond characteristics

Ponds were classified into three categories to characterise their hydrological connectivity and turbidity (e.g. Wessels et al., 2002; Takeuchi et al., 2012): 'isolated ponds' ($n = 6$) did not have inflows/outflows of water or ice cliffs; 'connected ponds without ice cliffs' ($n = 7$) were of higher turbidity and had inflows or outflows of water; and 'connected ponds with ice cliffs' ($n = 10$) were of highest turbidity, had inflows or outflows of water, and exhibited regular debris input due to ice cliff retreat. In this study, all ponds with ice cliffs had hydrological connectivity beyond their individual basins, although we note that this may not always be the case. Similarly, ponds may transition from one classification to another. The pond classification can generally be recognised by characteristic colours: isolated ponds were either green or clear, ponds connected without ice cliffs were turquoise, and ponds connected with ice cliffs were grey.

Hereon, ponds are referred to by their ID number (Figure 1), prefixed by 'K' for ponds on Khumbu Glacier or 'L' for ponds on Lobuche Glacier. The area and boundary of ponds was derived following Watson et al. (2016), by applying object-based image analysis (OBIA) classification applied to a panchromatic Pleiades satellite image (16th May 2016) followed by manual inspection and editing using corresponding multi-spectral imagery. All bathymetric surveys were conducted within 14 days of this image, hence we assumed that pond area did not change within this interval. However, pond boundaries buffered by one pixel were used in an uncertainty assessment described in the next section.

Supraglacial pond bathymetry

Sonar depth measurements collected by the USV were interpolated using the Natural Neighbour algorithm in ArcGIS, which preserves the values of measurement points, to derive the bathymetry for each supraglacial pond. Interpolated depths were gridded at 0.5 m resolution and forced to zero at the pond boundary derived from the Pleiades imagery, other than where an ice cliff was present, since cliffs are associated with pond deepening (Miles et al. 2016; Watson et al. in press). The surface area and volume of each pond were used to derive a power-law area-volume relationship. We performed a leave-one-out analysis to assess the uncertainty when deriving pond volumes using this area-volume relationship. Here, the area and volume of individual ponds were omitted from the dataset and an updated area-volume relationship was derived. We then used this updated relationship to predict the omitted pond's volume and assess the difference compared to the volume predicted using the original relationship (i.e. with the complete pond dataset). Uncertainties in pond area and volume were derived from 1000 Monte Carlo simulations of pond area and volume for each pond. Here, a Gaussian error model with a standard deviation equal to 3 % of the maximum pond depth (based on the sonar sensor uncertainty) was added to interpolated pond bathymetries using pond extents derived from the Pleiades satellite image (500 simulations), and these same pond extents with a one pixel buffer (500 simulations). These buffered pond extents represented potential pond expansion in the 14 day interval between the acquisition of the satellite image, and the final bathymetric surveys. Each simulation produced an estimate of pond area and volume, and the uncertainties reported in Table 2 represent one standard deviation of the 1000 simulations.

To investigate the spatial relationship between water depth and ice cliff presence, we generated sub samples of pond depth for all ponds with and without ice cliffs present. For ponds without an ice cliff present, polygonal buffers were generated from the pond shorelines at 0–5 m and 5–10 m. For ponds with an ice cliff present, polygonal buffers were also generated from pond shorelines at 0–5 m and 5–10 m, and additional buffers of the same distance were generated from the shoreline bounded by ice cliffs. These buffers were used to extract depth measurements using both the raw data points and interpolated pond bathymetry. Pair-wise Mann-Whitney U tests were then used to test for differences between each subsample of depth measurements.

Supraglacial pond instrumentation and monitoring

Ibutton thermistors (DS1922L-F5, number (n) = 18, with a manufacturer's stated accuracy $\pm 0.5^\circ$) were deployed in eight supraglacial ponds in October 2015 to monitor the thermal regime for one year, with a recording frequency of 60 minutes. Thermistors were shielded in a metal casing and deployed on a string, with one sensor floating at the pond surface attached below a floating buoy and one anchored at the bed by a weight. The strings were reset after downloading data in May 2016 where despite a clear water level rise for several ponds, the buoys remained at the surface due to slack left in the system. Therefore, we expect the top sensors were within 20 cm of the surface at all times. Pond K12 had two thermistor strings, one near an inlet to the pond and one near an ice cliff. Water level change was recorded at three ponds which captured different pond characteristics and drainage regimes (K9, K19, K18/21) using Solinst Levellogger Junior Edge pressure transducers.

Thermistors and pressure transducers were calibrated in a controlled temperature environment, revealing a maximum deviation of $\pm 0.22^\circ\text{C}$, which was within the

manufacturer's stated accuracy of $\pm 0.5^{\circ}\text{C}$. Individual temperature calibrations were applied to the field data based on the mean deviation from one thermistor used as a reference logger located in pond K9. Pressure transducers were barometrically compensated using data from the Barologger to report the water level change in ponds K9, K19 and K18/21. Here, water level refers to depth of water above the pressure transducer, which was not the point of maximum pond depth for K9 and K18/21, but was for K19.

Ponds K18/21 and K9 were turbid, with ice cliffs present, and had englacial (K18/21) and supraglacial (K9) drainage outlets. Pond K19 appeared less turbid and did not have an ice cliff present. The pressure transducer in the channel connecting K18/21 was withdrawn in May 2016 following entrapment on the bed. A Barologger Edge was deployed on Khumbu Glacier, which was shielded from solar radiation and recorded 1 m above-ground temperature and atmospheric pressure, for correction of the pond data.

We used corresponding pond bathymetry and water level data to derive a volumetric time-series for ponds K9 and K19. This was derived by simulating pond drainage at 20 cm increments and calculating the remaining pond area and volume for each iteration. Polynomial trend lines were fitted to area-volume scatter plots and the relationship was used to estimate the pond volume for each water level measurement. This was not possible for K18/21, since the pressure transducer became exposed and was withdrawn before bathymetry was collected in May 2016. Supraglacial pond drainage was simulated for all ponds with bathymetry data to derive individual area-volume relationships. Finally, study pond catchments were derived using ArcHydro Tools in ArcGIS and the circularity of pond boundaries was calculated using:

$$\text{Circularity} = \frac{P^2}{4\pi A} \quad (1)$$

where P and A are pond perimeter (m) and area (m^2) respectively. A circle would have a score of one.

Results

Supraglacial pond bathymetry and volume

The area of supraglacial ponds ranged from 39 m^2 (K14. Maximum depth of 1.3 m) to $18,744 \text{ m}^2$ (K21. Maximum depth of 45.6 m) with interpolated volumes of 24 m^3 and $290,928 \text{ m}^3$ respectively (Table 2). K21 was also the deepest pond at 45.6 m. Surveyed ponds had a total volume of $407,214 \pm 2908 \text{ m}^3$ and $92,020 \pm 680 \text{ m}^3$ on Khumbu and Lobuche Glaciers respectively. The water volume on Lobuche Glacier represents the total visible surface water storage since all supraglacial ponds were surveyed, whereas an estimated 26% of total pond area was surveyed on Khumbu Glacier.

The bathymetric data revealed that ponds rapidly deepen from the shoreline into one or more distinct basins (Figure 3). The maximum pond depths for connected ponds with an ice cliff, connected ponds without an ice cliff, and isolated ponds, were 45.6 m (K21), 13.5 m (K18), and 9.9 m (K2) respectively. Hydrologically-isolated ponds tended to be more circular in shape (mean circularity 1.50 ± 0.40) when compared to connected ponds with or without ice cliffs (mean circularity 2.54 ± 0.50) (Table 2), which had elongated or multiple basins (e.g. Figure 3f, g). Despite being initially classified as an isolated pond, an ice cliff appeared at the southern margin of K6 over the summer monsoon and the water level had dropped $\sim 1 \text{ m}$ between May–October 2016. Therefore, the pond classifications used in this study are not exclusive and ponds may transition between classes. Connected ponds with ice cliffs

were generally deeper in areas adjacent to the cliff faces and there was no evidence of an ice ramp protruding from any of the faces (e.g. Figure 3b, c, d). However, this was less apparent for several smaller ice cliffs (e.g. Figure 3a) or those bounded by areas of slumping debris, where pond depth increased more gradually from the shoreline.

We analysed the spatial variation in pond bathymetry using two shoreline buffers (0–5 m and 5–10 m) for groups of ponds with and without ice cliffs (Figure 4). The buffers for ponds with ice cliffs were split into cliff and non-cliff shoreline zones. Considering pond depth characteristics using the raw data points (e.g. Figure 2c), for ponds with ice cliffs, the area of pond 5–10 m from the ice cliff face had the highest median and mean depth (4.70 and 7.62 m respectively) (Figure 4). The median depth 0–5 m from ice cliffs (4.00 m) was significantly deeper than the median depth 0–5 m from non-cliff shorelines (1.60 m) (pair-wise Mann-Whitney U test, $p < 0.05$). Considering the non-cliff shoreline of ponds with and without ice cliffs, the 5–10 m zones were statistically different although this difference was small (median depths of 3.40 m and 3.70 m respectively). Pond depth comparisons using the interpolated pond bathymetry were similar to those using the raw data points, but generally of shallower depth (Supplementary Figure 1).

Area-volume relationships

The area and volume of surveyed supraglacial ponds in this study followed a power-law trend with a strong positive correlation ($R^2 = 0.98$) (Figure 5a); however, connected ponds with ice cliffs displayed greatest variability. The observed power-law relationship was comparable to that for the compiled dataset of Cook and Quincey (2015) and effectively extended the coverage for supraglacial ponds by three orders of magnitude (Figure 5b). When comparing the area-volume data points

during simulated pond drainage ($n = 761$), the gradient of the power-law increased and had a slightly lower R^2 of 0.97 (Figure 5c). The calculated area-volume relationship for K6 and K20 highlighted the effects of variable pond geometry (Figure 5d). K6, which had a regular shoreline and simple geometry draining into a central basin (Figure 3i), had a good fit to the power-law (Figure 5d). In contrast, K20 (Figure 3c) had an irregular shoreline and featured high-depth areas adjacent to an ice cliff, which had greater deviation from the power-law (Figure 5d). The ability to predict an individual pond volume V (m^3) using area A (m^2) using the power law (Equation 2) was not related to pond size (Supplementary Figure 2), and instead likely reflects variable pond morphologies. The mean difference between pond volumes calculated using the bathymetry and predicted pond volumes was 22.8%, or 18.5% with an outlier (K21) removed. Based on the addition of the new data from our study, the modified area-volume relationship of Cook and Quincey (2015) becomes:

$$V = 0.1535A^{1.39} \quad (2)$$

from the original:

$$V = 0.2A^{1.37} \quad (3)$$

The percentage differences between volumes predicted using the new versus old equation ranged from 7% (K21) to 19% (K14). We also note that the pond with an ice cliff studied by Miles et al. (2016a) on Lirung Glacier, Nepal, had an area of 650 m^2 and estimated volume of 1250 m^3 , which is accurately predicted by Equation (2) as 1245 m^3 .

Supraglacial pond thermal regime and drainage events

After deployment of the pressure transducer in October 2015, the water level at K19, which was connected without an ice cliff, gradually increased before stabilising December 2015 to March 2016 (Figure 6a). The water level started to rise in the first two weeks of April 2016 and the diurnal temperature range increased. The water level reached a peak on the 20th June 2016 at 7.1 m with an estimated volume of 3,145 m³. The water level then decreased gradually until the 18th July 2016. Subsequent drainage occurred 19th–25th July 2016 from a water level of ~6.4 m to ~3.4 m, which corresponded to an estimated 2,106 m³ decrease in volume. Diurnal temperature range increased following this drainage (Figure 6a). The final drainage event began 10th–11th September 2016 and the water level was zero by 22:00 on the 12th September 2016. Notably, the drainage event initiated on the 19th July 2016 was coincident with a rapid temperature rise in the neighbouring pond K20 (Supplementary Figure 3), which we interpret as a coincident drainage event exposing the temperature logger to the atmosphere. K20 was not instrumented with a pressure transducer but field observations confirmed complete drainage by the start of October 2016.

The water level of K9, which was connected and with several ice cliffs, decreased during winter until ~20th March 2016 (Figure 6b). The water level then increased during summer reaching peaks on the 12th July 2016 (5.5 m) and 21st August 2016 (5.7 m) before decreasing throughout September 2016. The rising and falling limbs both include a diurnal temperature cycle, but not a diurnal water level fluctuation. The initial and final water level of K9 were comparable (4.6 m on 22nd October 2015 and 4.1 m on 6th October 2016). Notably, the water level of K18/21 also decreased

during the ~1 month of observations in winter, and was also apparent from slumped ice plates around the margin of the pond (Figure 6c).

The absolute temperature of K9 was lower than K19; however, the diurnal temperature variation was greatest for K9 with a summer variation of ~0.5°C (Figure 7). In contrast, the summer diurnal temperature variation for K19 was ~0.2°C. There was evidence of a subdued winter diurnal temperature cycle in K9 but not in K19; however, the water temperature remained above 4°C in K19 during winter.

Three complete pond drainage events were observed over the study period at K19, K20, and K22. The potential internal glacier ablation resulting from pond drainage through downstream ice M_i , assuming a temperature drop to 0°C, can be estimated using Equation (4) (e.g. Thompson et al., 2016):

$$M_i = M_w \Delta T \left(\frac{C}{L} \right) \quad (4)$$

where M_w is the water mass, ΔT indicates the difference in temperature between observed and zero, C the specific heat capacity of water (4.2 kJ kg⁻¹ k⁻¹) and L the latent heat of melting (344 kJ kg⁻¹ k⁻¹). For ΔT we used the median of the mean surface and bottom temperatures of the day prior to drainage. Measurement uncertainties in pond temperature ($\pm 0.5^\circ\text{C}$) and volume (Table 2) were used to derive a confidence interval when calculating the englacial ablation potential of drained ponds. The drainage of K22 with a water mass of $1634 \pm 28 \times 10^3$ kg and temperature change 10.3 ± 0.5 °C had an englacial ablation potential of $203 \pm 14 \times 10^3$ kg. The drainage of K20 with a water mass of $13369 \pm 163 \times 10^3$ kg and a temperature change of 2.9 ± 0.5 °C had an englacial ablation potential of $473 \pm 88 \times 10^3$ kg. The drainage of K19 with a water mass of $2116 \pm 66 \times 10^3$ kg and

temperature change of 4.0 ± 0.5 °C had an englacial ablation potential of $103 \pm 17 \times 10^3$ kg.

Pond temperature

The mean water temperature of isolated ponds and connected ponds without ice cliffs, was greater than connected ponds with ice cliffs (Figure 8). Mean bottom water temperatures for connected ponds with ice cliffs ranged from 0.1 to 0.5°C for winter and 0.2 to 2.0°C for summer. In contrast, the mean bottom water temperatures for isolated and connected ponds without ice cliffs ranged from 4.1 to 5.0°C for winter and 4.2 to 9.8°C for summer. Summer surface water temperatures were comparable to summer bottom water temperatures, suggesting that ponds were well mixed. The greatest difference in mean summer surface and bottom water temperature was 1.2°C for K13. Winter surface temperatures were distinctly different from the winter bottom water temperatures for five ponds (K12, K23, K19, K13, K22), suggesting that temperature loggers became frozen in a layer of ice over winter, which was supported by field observations. K9 had an inflow and outflow of water and was largely ice-free on 22nd October 2015, but had developed a surface layer of ice ~10 cm thick by 11th November 2015. Other ponds without hydrological connectivity were observed to be freezing over upon arrival into the field on 20th October 2015.

Discussion

Supraglacial pond bathymetry

Our data contribute to a sparse bathymetry dataset of supraglacial ponds on Himalayan debris-covered glaciers, which is due to the significant effort that is required to make distributed depth measurements. Point measurements of pond or lake depths are usually made using a sonar after cutting through the frozen surface

(Benn et al., 2001); directly through the frozen surface using sonar (Thompson et al., 2012); from a boat (Rohl, 2008; Somos-Valenzuela et al., 2014b); or more recently using ground-penetrating radar (GPR) (Mertes et al., 2016), which provides additional information on basal sediment. The spatial resolution of surveys can be increased when using an USV (Horodyskyj, 2015), which also allows sampling close to ice cliffs where falling debris would otherwise restrict safe access.

Hydrologically-isolated ponds without ice cliffs were located along the western margin of Khumbu Glacier, which is stagnant and supporting some scrub vegetation in parts (Inoue and Yoshida, 1980); however, the sub-debris ice content is unknown. These isolated ponds often exhibited a green appearance due to algal growth and low turbidity (Takeuchi et al., 2012), and were generally smaller and shallower than the other ponds surveyed. However, isolated ponds K2 and K6 had depths of 9.9 m and 9.1 m respectively (Table 2). Notably, an ice cliff developed along the margin of K6 and the water level dropped by over 1 m during the 2016 summer monsoon. Pond K6 was identified by Iwata et al. (1980) in 1978 and has persisted in a similar shape with little change in areal extent (Watson et al., 2016). It is not clear whether a degrading ice core in this area will lead to further drainage. Nonetheless, it indicates that apparently stable ponds on stagnant parts of the glacier may still be actively deepening towards the hydrological base level.

Connected ponds with ice cliffs had the greatest depths and often elongated or multiple basins (Figure 3). The greatest measured depth was 45.6 m at K21, which is located in an area of maximum ice thickness of ~100 m (Gades et al., 2000). The maximum depth was observed adjacent to a large ice cliff (Figure 3d), similar to observations by Thompson et al. (2016) and Horodyskyj (2015) on Ngozumpa Glacier, who observed maximum depths of 27 m and 54 m close to ice cliffs. Miles et

al. (2016a) observed linearly increasing pond depth approaching an ice cliff on Lirung Glacier, although depth measurements were limited due to rockfall hazard. Whilst pond depth generally increased approaching large ice cliff faces in our observations (Figure 3), this was not the case for many smaller ice cliffs or those in areas of slumping debris. This variability led to highest depth observations in areas 5–10 m from cliff faces (Figure 4). Shallower pond depth around small ice cliffs likely reflects newly exposed cliff faces or areas where thick subaqueous debris cover due to slumping restricts basal melt (Mertes et al., 2016). In contrast, larger cliff faces develop and persist where subaqueous thermal erosion matches or exceeds subaerial melt or calving (Benn et al., 2001; Sakai et al., 2009). Here, rapid cliff retreat limits debris accumulation at the cliff base and hence it is likely that subaqueous melt of the cliff and pond bed promotes deepening approaching the cliff face. Therefore, the bathymetry of ponds with ice cliffs indicates whether pond expansion is likely, and hence the evolutionary trajectory of the cliff-pond coupling.

Area-volume relationships

We have derived a new empirical area-volume relationship by extending the dataset of Cook and Quincey (2015), through measuring the bathymetry of 24 supraglacial ponds on two debris-covered glaciers not included in their original analysis. Watson et al. (2016) found that individual ponds $<3,600 \text{ m}^2$ made up 48–88% of pond area on nine debris-covered glaciers in the Everest region, which is well represented by the range of ponds in this study ($39\text{--}18,744 \text{ m}^2$), but was not represented in existing datasets (Cook and Quincey, 2015). All surveyed ponds followed a power-law relationship between area and volume (Figure 5a); however, ponds with ice cliffs displayed greatest deviation from this trend, owing to the prevalence of deep zones adjacent to ice cliffs (e.g. K21 Figure 3d), or to elongated irregular shaped basins

(e.g. K12). This variable morphology was apparent when using a power law to predict individual pond volumes (Supplementary Figure 2), where the mean difference between the pond volume and predicted pond volume was 22.8%, or 18.5% with an outlier (K21) removed. An even larger bathymetric dataset would further refine empirical area-volume relationships and facilitate further analysis of ponds of variable ice cliff presence, different hydrological connectivity, and at different stages of development. However, it is clear that area-volume relationships derived from predominantly proglacial lakes can be extended to smaller ponds.

A mean of ~50% of ice cliffs featured a supraglacial pond in the Everest region (Watson et al., 2017), therefore around half of all pond morphologies are expected to be highly dynamic due to ice cliff retreat. In contrast, subaqueous sub-debris melt rates and therefore geometry changes are expected to be low for those without ice cliffs (Miles et al., 2016a). Multi-temporal supraglacial pond bathymetry data are therefore required to assess pond evolution and the trajectory of proglacial lake development. Simulating pond drainage increased the number of area-volume data points (Figure 5C) and was used to reconstruct volume change, which is useful to assess the seasonal water storage of ponds. However, these represent a snapshot of pond bed morphology and do not reveal anything about its genesis.

Supraglacial pond drainage and thermal regime

Supraglacial ponds display considerable inter- and intra-annual variation in their surface area (Miles et al., 2016b; Watson et al., 2016), including evidence of a seasonal peak related to the onset of the ablation season with the Indian Summer Monsoon in June (Liu et al., 2015; Miles et al., 2016b; Narama et al., 2017). The observed hydrological regime of ponds K19 and K9 displayed a seasonal trend and water levels peaked in late June and early July 2016 respectively (Figure 6a, b). The

water level of K9 dropped slightly before a secondary peak on the 21st August. K9 had both an inflow and outflow of water and formed part of a connected series of ponds on the easterly margin of Khumbu Glacier (Figure 1b). Therefore, the seasonal water level peak of this pond reflects maximum meltwater generation during the monsoon, before the water level began to drop in late August 2016.

The sporadic drainage of K19 was likely due to the interception and enlargement of an englacial conduit, which drained most of the pond and was more rapid than the gradual seasonal expansion and drainage observed at K9. The main drainage event at K19 occurred 19th–25th July 2016; however, the water level of the pond began to drop gradually several days prior to this. Notably, the adjacent pond K20 also appeared to drain on the 19th July 2016, inferred by the aerial exposure of the temperature logger (Supplementary Figure 3). The temperature of K19 rose from 4°C to 5.5°C within 24 hours during this drainage event (Figure 6a), which may be due to greater local radiation heating as the pond volume decreased. K20 had a lower temperature (~3°C), although it appears likely that both ponds exploited the same englacial conduit to drain and hence developed a sub-surface connection. It is clear that ponds in close proximity are likely to exhibit or develop sub-surface connections that are not apparent from surface observations. Notably, the timing and connectivity of these ponds is also consistent with the observations of Narama et al. (2017), who also observed englacial drainage for June-July for supraglacial ponds in the Tien Shan Mountains.

Water temperatures of ponds with ice cliffs ($n = 6$) were generally close to zero degrees Celsius and featured a frozen surface during winter, and summer surface temperatures did not exceed 4.2°C (Figure 8). The pond monitored by Xin et al. (2012) also had an ice cliff present but was located at ~1685 m lower elevation and

had an average summer surface temperature of 9.0°C. The pond with an ice cliff monitored by Miles et al. (2016a) at an elevation of 4070 m had an average temperature of 1–1.5°C and was more comparable to our study ponds. From surveys of ponds on debris-covered glaciers in Nepal, Sakai et al. (2009) revealed that subaqueous melt exceeds subaerial ice cliff melt at ponds with a water temperature of 2–4°C and a fetch of >20m, and that a fetch >~80 m is required for calving. During our study, full-slab calving was observed at K15 and block calving was apparent prior to K12 being instrumented in October 2015 (Supplementary Figure 4). These ice blocks at K12 had melted by May 2016. The ponds had fetches of ~35 m and ~140 m respectively, estimated following Sakai et al. (2009). The temperature at K15 was not recorded but the basin was connected to K12, which had a mean temperature of <1°C, and hence did not meet the expected calving criteria. We note that Sakai et al. (2009) also observed a calving cliff with a pond temperature of less than <1°C on Khumbu Glacier, but with a larger fetch of 94 m. It is likely that the higher turnover of water into K15 via an inlet, promoted thermal undercutting and calving despite the small fetch. The role of water inflows should therefore be considered alongside wind-driven currents in the energy-balance modelling of supraglacial ponds (e.g. Miles et al., 2016a).

The temperature of isolated ponds was notably higher than those with ice cliffs, and all had mean temperatures >4°C at the pond bed over winter, suggesting that their thermal energy was stored over winter, insulated by a layer of snow-covered ice (Figure 8). Ponds K19, K20, and K22 drained over the study period with englacial ablation potentials of $103 \pm 17 \times 10^3$ kg, $473 \pm 88 \times 10^3$ kg, and $203 \pm 14 \times 10^3$ kg respectively. Notably K20 had the greatest englacial ablation potential despite having the lowest temperature (1.8°C), due to its volume. These values only represent

englacial ablation due to drainage without considering the turnover of water through each pond during their lifespan. Nonetheless, our observations support the role of seasonal pond dynamics acting as a notable source of glacier ablation (Miles et al., 2016a).

Implications of seasonal pond dynamics

Through revealing short-term supraglacial pond dynamics on two Himalayan debris-covered glaciers, our study adds further evidence to support observations of cyclical pond growth and drainage due to ablation and precipitation input during the summer monsoon, followed by winter freezing of the pond surface, which subdues or inhibits diurnal temperature cycles. However, we observed ponds continuing to drain throughout winter (e.g. K9 and K18/K21), suggesting that the hydrological system and hence englacial ablation remained active at this time. Sporadic drainage events are imposed on the seasonal cycle of pond expansion as ponds intercept englacial conduits and stored thermal energy is transmitted englacially, contributing notably to glacier-scale ablation (Sakai et al., 2000; Miles et al., 2016a). Additionally, meltwater was conveyed through ponds by a network of supraglacial and englacial channels (e.g. K15), which leads to a high overturning rate conducive to the undercutting and calving of adjacent ice cliffs (Sakai et al., 2009; Miles et al., 2016a).

Our observations of glacier surface hydrology in the lower ablation zone suggest that seasonal pond expansion and drainage was linked to meltwater generation from glacier ablation; however, this seasonal trend was occasionally interrupted by sporadic short-term drainage events, where ponds intercepted an englacial conduit. These conduits become enlarged when supporting a drainage event and grade towards the hydrological base level, and may support multiple drainage events in between periods of dormancy (Gulley and Benn, 2007; Gulley et al., 2009; Benn et

al., 2009). In this study we investigated the potential englacial ablation from draining ponds; however, the quantity and ablative role of water stored in blocked englacial conduits remains unknown. Englacial water storage likely also responds to seasonal ablation processes driving meltwater generation, which is stored and released during outburst flood events (e.g. Rounce et al., 2017b) or buffered by the internal drainage system for larger low-gradient glaciers. In the upper ablation zone of debris-covered glaciers, observations of increased summer velocities on Lirung and Ngozumpa Glaciers, suggest that basal-sliding is promoted where surface meltwater is routed to the glacier bed (e.g. via crevasses) (Kraaijenbrink et al., 2016; Benn et al., 2017). Seasonal velocity observations are lacking for Khumbu Glacier; however, it is likely that surface-bed hydrological connections play a similar role.

Knowledge of short-term pond dynamics and evolution as presented in this study allows a greater understanding of their potential role for glacier-scale ablation, in addition to developing future links between observed mass loss and the meltwater budget. Several key lines of enquiry should be pursued to better constrain the role of the pond-cliff interaction for glacier-wide ablation, and to quantify seasonal meltwater fluxes, which will become increasingly important as the reservoirs of freshwater locked in glaciers decline over the coming century:

- (1) Observations of pond dynamics throughout the summer monsoon with high temporal resolution optical or SAR imagery could be used in association with empirical area-volume relationships to predict water fluxes.
- (2) Distributed instrumentation of ponds on other debris-covered glaciers combined with pond energy balance modelling (e.g. Miles et al., 2016a) would allow a spatio-temporal assessment of pond thermal regimes and water level

fluctuations, which could be used to model their total contribution to glacier-scale ablation.

(3) Multi-temporal pond bathymetry is required to quantify expansion processes related to ice cliff retreat or debris infilling (e.g. Thompson et al., 2016; Mertes et al., 2016), and to better understand the interface between the thickness of basal sediment and glacier ice, which has a large influence on subaqueous melt rates.

Conclusions

A spatially distributed bathymetric survey of supraglacial ponds has extended the compiled dataset of Cook and Quincey (2015), to determine an empirical relationship between pond area and volume for the size-distribution of ponds commonly encountered on Himalayan debris-covered glaciers. We revealed evidence of pond deepening in association with the presence of ice cliffs up to a depth of 45.6 m, which supports observations of thermal undercutting and their role as hot-spots of melt on debris-covered glaciers. Downward grading of the pond bed in association with ice cliff retreat is likely to promote ice cliff persistence (Watson et al., in press), and a contrasting evolutionary trajectory compared to ponds without ice cliffs. The water temperatures of ponds with ice cliffs ($n = 6$) were generally close to zero degrees Celsius, and summer surface temperatures did not exceed 4.2°C. The temperature of hydrologically isolated ponds was notably higher and all had mean temperatures >4 °C at the pond bed over winter, suggesting that their thermal energy is stored over winter, trapped in by an insulating layer of snow-covered ice.

Seasonal expansion and drainage of ponds was observed, which supports satellite remote sensing observations (Liu et al., 2015; Miles et al., 2016b; Watson et al., 2016). Continued pond drainage throughout winter suggests the hydrological system

and therefore englacial ablation remains at least partially active through the year. Sporadic drainage events were imposed on this seasonal cycle as ponds intercepted englacial conduits and transferred their stored thermal energy englacially. Increased meltwater generation during the summer monsoon is also likely to be expressed through englacial water storage and release (Rounce et al., 2017b), in addition to conduit enlargement and collapse, leading to the formation of new surface depressions and ice cliffs.

Acknowledgements

We thank Wojciech Marcinek, Daniel Hicks, Adil Tahir, and Charles Howard for designing and building the USV ('BathyBot') within the School of Mechanical Engineering at the University of Leeds, and Robert Richardson and Shaun Whitehead for their guidance on the project. C.S.W acknowledges fieldwork support from the School of Geography at the University of Leeds, the Mount Everest Foundation, the British Society for Geomorphology, the Royal Geographical Society (with IBG), the Petzl Foundation, and water@leeds. Advanced Elements Kayaks are thanked for a PackLite kayak and Pascal Buri for an earlier dinghy, which enabled pond access. The Natural Environment Research Council Geophysical Equipment Facility is thanked for loaning Global Navigation Satellite Systems receivers and for technical assistance under loan numbers 1050, 1058, and 1065. The Pleiades satellite images was supplied by the European Space Agency under Category-1 Proposal Id. 32600. Dhananjay Regmi and Himalayan Research Expeditions are thanked for fieldwork support and research permit acquisition. Mahesh Magar is thanked for invaluable help collecting data during the three field campaigns. Ian Willis and one anonymous reviewer are thanked for thorough and constructive reviews, which helped improve this study.

References

- Benn, D Gulley, J Luckman, A Adamek, A and Glowacki, PS. 2009. Englacial drainage systems formed by hydrologically driven crevasse propagation. *Journal of Glaciology* **55**: 513-523.
- Benn, DI Bolch, T Hands, K Gulley, J Luckman, A Nicholson, LI Quincey, D Thompson, S Toumi, R and Wiseman, S. 2012. Response of debris-covered glaciers in the Mount Everest region to recent warming, and implications for outburst flood hazards. *Earth-Science Reviews* **114**: 156-174.
<http://dx.doi.org/10.1016/j.earscirev.2012.03.008>
- Benn, DI Thompson, S Gulley, J Mertes, J Luckman, A and Nicholson, L. 2017. Structure and evolution of the drainage system of a Himalayan debris-covered glacier, and its relationship with patterns of mass loss. *The Cryosphere Discuss.* **2017**: 1-43. 10.5194/tc-2017-29
- Benn, DI Wiseman, S and Hands, KA. 2001. Growth and drainage of supraglacial lakes on debris-mantled Ngozumpa Glacier, Khumbu Himal, Nepal. *Journal of Glaciology* **47**: 626-638. 10.3189/172756501781831729
- Biggs, J Williams, P Whitfield, M Nicolet, P and Weatherby, A. 2005. 15 years of pond assessment in Britain: results and lessons learned from the work of Pond Conservation. *Aquatic Conservation: Marine and Freshwater Ecosystems* **15**: 693-714. 10.1002/aqc.745
- Bolch, T Pieczonka, T and Benn, DI. 2011. Multi-decadal mass loss of glaciers in the Everest area (Nepal Himalaya) derived from stereo imagery. *The Cryosphere* **5**: 349-358. 10.5194/tc-5-349-2011
- Box, JE and Ski, K. 2007. Remote sounding of Greenland supraglacial melt lakes: implications for subglacial hydraulics. *Journal of Glaciology* **53**: 257-265. 10.3189/172756507782202883
- Carrivick, JL and Tweed, FS. 2013. Proglacial lakes: character, behaviour and geological importance. *Quaternary Science Reviews* **78**: 34-52.
<http://dx.doi.org/10.1016/j.quascirev.2013.07.028>
- Carrivick, JL and Tweed, FS. 2016. A global assessment of the societal impacts of glacier outburst floods. *Global and Planetary Change* **144**: 1-16.
<http://dx.doi.org/10.1016/j.gloplacha.2016.07.001>
- Cook, SJ and Quincey, DJ. 2015. Estimating the volume of Alpine glacial lakes. *Earth Surf. Dynam.* **3**: 559-575.
- Fujita, K Sakai, A Nuimura, T Yamaguchi, S and Sharma, RR. 2009. Recent changes in Imja Glacial Lake and its damming moraine in the Nepal Himalaya revealed by in situ surveys and multi-temporal ASTER imagery. *Environmental Research Letters* **4**: 1-7. 10.1088/1748-9326/4/4/045205
- Gades, A Conway, H and Nereson, N. 2000. Radio echo-sounding through supraglacial debris on Lirung and Khumbu Glaciers, Nepal Himalayas. In: *IAHS Publ. 264 (Symposium at Seattle 2000 – Debris-Covered Glaciers), Seattle, Washington, U.S.A.* IAHS Publication.
- Gardelle, J Arnaud, Y and Berthier, E. 2011. Contrasted evolution of glacial lakes along the Hindu Kush Himalaya mountain range between 1990 and 2009. *Global and Planetary Change* **75**: 47-55.
<http://dx.doi.org/10.1016/j.gloplacha.2010.10.003>

- Gulley, J and Benn, DI. 2007. Structural control of englacial drainage systems in Himalayan debris-covered glaciers. *Journal of Glaciology* **53**: 399-412. 10.3189/002214307783258378
- Gulley, JD Benn, DI Sreaton, E and Martin, J. 2009. Mechanisms of englacial conduit formation and their implications for subglacial recharge. *Quaternary Science Reviews* **28**: 1984-1999. 10.1016/j.quascirev.2009.04.002
- Horodyskyj, U. 2015. *Contributing Factors to Ice Mass Loss on Himalayan Debris-covered Glaciers*. PhD thesis, University of Colorado, Boulder.
- Immerzeel, WW Kraaijenbrink, PDA Shea, JM Shrestha, AB Pellicciotti, F Bierkens, MFP and de Jong, SM. 2014. High-resolution monitoring of Himalayan glacier dynamics using unmanned aerial vehicles. *Remote Sensing of Environment* **150**: 93-103. 10.1016/j.rse.2014.04.025
- Inoue, J and Yoshida, M. 1980. Ablation and heat exchange over the Khumbu glacier. *Journal of the Japanese Society of Snow and Ice* **39**: 7-14.
- Iwata, S, Watanabe, O. and Fushimi, H. 1980. Surface Morphology in the Ablation Area of the Khumbu Glacier. *Seppyo*, 41 (Special issue) **9-17**.
- Kattelman, R. 2003. Glacial lake outburst floods in the Nepal Himalaya: A manageable hazard? *Natural Hazards* **28**: 145-154. 10.1023/a:1021130101283
- Kirkbride, MP. 1993. The temporal significance of transitions from melting to calving termini at glaciers in the central Southern Alps of New Zealand. *The Holocene* **3**: 232-240. 10.1177/095968369300300305
- Komori, J. 2008. Recent expansions of glacial lakes in the Bhutan Himalayas. *Quaternary International* **184**: 177-186. <http://dx.doi.org/10.1016/j.quaint.2007.09.012>
- Kraaijenbrink, P Meijer, SW Shea, JM Pellicciotti, F de Jong, SM and Immerzeel, WW. 2016. Seasonal surface velocities of a Himalayan glacier derived by automated correlation of unmanned aerial vehicle imagery. *Annals of Glaciology* **57**: 103-113.
- Lamsal, D Sawagaki, T Watanabe, T and Byers, AC. 2016. Assessment of glacial lake development and prospects of outburst susceptibility: Chamlang South Glacier, eastern Nepal Himalaya. *Geomatics, Natural Hazards and Risk* **7**: 403-423. 10.1080/19475705.2014.931306
- Liu, Q Christoph, M and Shiyin, L. 2015. Distribution and interannual variability of supraglacial lakes on debris-covered glaciers in the Khan Tengri-Tumor Mountains, Central Asia. *Environmental Research Letters* **10**: 1-10.
- Mertes, JR Thompson, SS Booth, AD Gulley, JD and Benn, DI. 2016. A conceptual model of supraglacial lake formation on debris-covered glaciers based on GPR facies analysis. *Earth Surface Processes and Landforms* **42**: 903-914 10.1002/esp.4068
- Miles, ES Pellicciotti, F Willis, IC Steiner, JF Buri, P and Arnold, NS. 2016a. Refined energy-balance modelling of a supraglacial pond, Langtang Khola, Nepal. *Annals of Glaciology* **57**: 29-40.
- Miles, ES Willis, IC Arnold, NS Steiner, J and Pellicciotti, F. 2016b. Spatial, seasonal and interannual variability of supraglacial ponds in the Langtang Valley of Nepal, 1999-2013. *Journal of Glaciology* **63**: 1-18. 10.1017/jog.2016.120
- Miles, KE Willis, IC Benedek, CL Williamson, AG and Tedesco, M. 2017. Toward Monitoring Surface and Subsurface Lakes on the Greenland Ice Sheet Using

- Sentinel-1 SAR and Landsat-8 OLI Imagery. *Frontiers in Earth Science* **5**: 10.3389/feart.2017.00058
- Moussavi, MS Abdalati, W Pope, A Scambos, T Tedesco, M MacFerrin, M and Grigsby, S. 2016. Derivation and validation of supraglacial lake volumes on the Greenland Ice Sheet from high-resolution satellite imagery. *Remote Sensing of Environment* **183**: 294-303.
<http://dx.doi.org/10.1016/j.rse.2016.05.024>
- Naito, N Nakawo, M Kadota, T and Raymond, CF. 2000. Numerical simulation of recent shrinkage of Khumbu Glacier, Nepal Himalayas. In: Nakawo, M. Raymond, C.F. and Fountain, A., eds. *IAHS Publ. 264 (Symposium at Seattle 2000 – Debris-Covered Glaciers)*, Seattle, Washington, U.S.A. IAHS Publication, 245-254.
- Narama, C Daiyrov, M Tadono, T Yamamoto, M Kääh, A Morita, R and Ukita, J. 2017. Seasonal drainage of supraglacial lakes on debris-covered glaciers in the Tien Shan Mountains, Central Asia. *Geomorphology* **286**: 133-142.
<http://dx.doi.org/10.1016/j.geomorph.2017.03.002>
- Nicholson, L and Benn, DI. 2013. Properties of natural supraglacial debris in relation to modelling sub-debris ice ablation. *Earth Surface Processes and Landforms* **38**: 490-501. 10.1002/esp.3299
- Nie, Y Liu, Q and Liu, S. 2013. Glacial Lake Expansion in the Central Himalayas by Landsat Images, 1990–2010. *PLoS ONE* **8**: 1-8.
10.1371/journal.pone.0083973
- Nie, Y Sheng, Y Liu, Q Liu, L Liu, S Zhang, Y and Song, C. 2017. A regional-scale assessment of Himalayan glacial lake changes using satellite observations from 1990 to 2015. *Remote Sensing of Environment* **189**: 1-13.
<http://dx.doi.org/10.1016/j.rse.2016.11.008>
- Pellicciotti, F Stephan, C Miles, E Herreid, S Immerzeel, WW and Bolch, T. 2015. Mass-balance changes of the debris-covered glaciers in the Langtang Himal, Nepal, from 1974 to 1999. *Journal of Glaciology* **61**: 373-386.
- Pope, A Scambos, TA Moussavi, M Tedesco, M Willis, M Shean, D and Grigsby, S. 2016. Estimating supraglacial lake depth in West Greenland using Landsat 8 and comparison with other multispectral methods. *The Cryosphere* **10**: 15-27.
10.5194/tc-10-15-2016
- Purdie, H Bealing, P Tidey, E Gomez, C and Harrison, J. 2016. Bathymetric evolution of Tasman Glacier terminal lake, New Zealand, as determined by remote surveying techniques. *Global and Planetary Change* **147**: 1-11.
<http://dx.doi.org/10.1016/j.gloplacha.2016.10.010>
- Quincey, DJ Luckman, A and Benn, D. 2009. Quantification of Everest region glacier velocities between 1992 and 2002, using satellite radar interferometry and feature tracking. *Journal of Glaciology* **55**: 596-606.
- Quincey, DJ Richardson, SD Luckman, A Lucas, RM Reynolds, JM Hambrey, MJ and Glasser, NF. 2007. Early recognition of glacial lake hazards in the Himalaya using remote sensing datasets. *Global and Planetary Change* **56**: 137-152. <http://dx.doi.org/10.1016/j.gloplacha.2006.07.013>
- Ragettli, S Bolch, T and Pellicciotti, F. 2016. Heterogeneous glacier thinning patterns over the last 40 years in Langtang Himal, Nepal. *The Cryosphere* **10**: 2075-2097. 10.5194/tc-10-2075-2016
- Reynolds, JM. 2000. On the formation of supraglacial lakes on debris-covered glaciers. In: Nakawo, M. Raymond, C.F. and Fountain, A., eds. *IAHS Publ. 264*

- (*Symposium at Seattle 2000 – Debris-Covered Glaciers*), Seattle, Washington, U.S.A. IAHS Publishing, 153-161.
- Rohl, K. 2008. Characteristics and evolution of supraglacial ponds on debris-covered Tasman Glacier, New Zealand. *Journal of Glaciology* **54**: 867-880.
- Rounce, D Watson, C and McKinney, D. 2017a. Identification of hazard and risk for glacial lakes in the Nepal Himalaya using satellite imagery from 2000–2015. *Remote Sensing* **9**. doi:10.3390/rs9070654
- Rounce, DR Byers, AC Byers, EA and McKinney, DC. 2017b. Brief communication: Observations of a glacier outburst flood from Lhotse Glacier, Everest area, Nepal. *The Cryosphere* **11**: 443-449. 10.5194/tc-11-443-2017
- Rounce, DR McKinney, DC Lala, JM Byers, AC and Watson, CS. 2016. A new remote hazard and risk assessment framework for glacial lakes in the Nepal Himalaya. *Hydrol. Earth Syst. Sci.* **20**: 3455-3475. 10.5194/hess-20-3455-2016
- Sakai, A Nishimura, K Kadota, T and Takeuchi, N. 2009. Onset of calving at supraglacial lakes on debris-covered glaciers of the Nepal Himalaya. *Journal of Glaciology* **55**: 909-917.
- Sakai, A Takeuchi, N Fujita, K and Nakawo, M. 2000. Role of supraglacial ponds in the ablation process of a debris-covered glacier in the Nepal Himalayas. In: Nakawo, M. Raymond, C.F. and Fountain, A., eds. *IAHS Publ. 264 (Symposium at Seattle 2000 – Debris-Covered Glaciers)*, Seattle, Washington, U.S.A. IAHS Publishing, 119-130.
- Salerno, F Thakuri, S D'Agata, C Smiraglia, C Manfredi, EC Viviano, G and Tartari, G. 2012. Glacial lake distribution in the Mount Everest region: Uncertainty of measurement and conditions of formation. *Global and Planetary Change* **92-93**: 30-39. 10.1016/j.gloplacha.2012.04.001
- Shrestha, BB and Nakagawa, H. 2014. Assessment of potential outburst floods from the Tsho Rolpa glacial lake in Nepal. *Natural Hazards* **71**: 913-936. 10.1007/s11069-013-0940-3
- Somos-Valenzuela, MA McKinney, DC Byers, AC Rounce, DR Portocarrero, C and Lamsal, D. 2014a. Assessing downstream flood impacts due to a potential GLOF from Imja Lake in Nepal. *Hydrol. Earth Syst. Sci. Discuss.* **19**: 1401-1412. 10.5194/hessd-11-13019-2014
- Somos-Valenzuela, MA McKinney, DC Rounce, DR and Byers, AC. 2014b. Changes in Imja Tsho in the Mount Everest region of Nepal. *The Cryosphere* **8**: 1661-1671. 10.5194/tc-8-1661-2014
- Strozzi, T Wiesmann, A Kaab, A Joshi, S and Mool, P. 2012. Glacial lake mapping with very high resolution satellite SAR data. *Natural Hazards and Earth System Sciences* **12**: 2487-2498. 10.5194/nhess-12-2487-2012
- Sugiyama, S Minowa, M Sakakibara, D Skvarca, P Sawagaki, T Ohashi, Y Naito, N and Chikita, K. 2016. Thermal structure of proglacial lakes in Patagonia. *Journal of Geophysical Research: Earth Surface*: p2016JF004084. 10.1002/2016JF004084
- Takeuchi, N Sakai, A Kohshima, S Fujita, K and Nakawo, M. 2012. Variation in Suspended Sediment Concentration of Supraglacial Lakes on Debris Covered Area of the Lirung Glacier in the Nepal Himalayas. *Global Environmental Research* **16**: 95-104.
- Thakuri, S Salerno, F Smiraglia, C Bolch, T D'Agata, C Viviano, G and Tartari, G. 2014. Tracing glacier changes since the 1960s on the south slope of Mt.

- Everest (central Southern Himalaya) using optical satellite imagery. *Cryosphere* **8**: 1297-1315. 10.5194/tc-8-1297-2014
- Thompson, S Benn, D Mertes, J and Luckman, A. 2016. Stagnation and mass loss on a Himalayan debris-covered glacier: processes, patterns and rates. *Journal of Glaciology* **62**: 467-485. doi:10.1017/jog.2016.37
- Thompson, SS Benn, DI Dennis, K and Luckman, A. 2012. A rapidly growing moraine-dammed glacial lake on Ngozumpa Glacier, Nepal. *Geomorphology* **145**: 1-11. 10.1016/j.geomorph.2011.08.015
- Wang, WC Xiang, Y Gao, Y Lu, AX and Yao, TD. 2015. Rapid expansion of glacial lakes caused by climate and glacier retreat in the Central Himalayas. *Hydrological Processes* **29**: 859-874. 10.1002/hyp.10199
- Watanabe, T Ives, JD and Hammond, JE. 1994. Rapid Growth of a Glacial Lake in Khumbu Himal, Himalaya: Prospects for a Catastrophic Flood. *Mountain Research and Development* **14**: 329-340. 10.2307/3673729
- Watson, CS Quincey, DJ Carrivick, JL and Smith, MW. 2016. The dynamics of supraglacial ponds in the Everest region, central Himalaya. *Global and Planetary Change* **142**: 14-27.
<http://dx.doi.org/10.1016/j.gloplacha.2016.04.008>
- Watson, CS Quincey, DJ Carrivick, JL and Smith, MW. 2017. Ice cliff dynamics in the Everest region of the Central Himalaya. *Geomorphology* **278**: 238-251.
<http://dx.doi.org/10.1016/j.geomorph.2016.11.017>
- Watson, CS Quincey, DJ Smith, MW Carrivick, JL Rowan, AV and James, M. *In press*. Quantifying ice cliff evolution with multi-temporal point clouds on the debris-covered Khumbu Glacier, Nepal. *Journal of Glaciology*.
- Wessels, RL Kargel, JS and Kieffer, HH. 2002. ASTER measurement of supraglacial lakes in the Mount Everest region of the Himalaya. *Annals of Glaciology* **34**: 399-408. 10.3189/172756402781817545
- Xin, W Shiyin, L Haidong, H Jian, W and Qiao, L. 2012. Thermal regime of a supraglacial lake on the debris-covered Koxkar Glacier, southwest Tianshan, China. *Environmental Earth Sciences* **67**: 175-183. 10.1007/s12665-011-1490-1
- Zhang, G Yao, T Xie, H Wang, W and Yang, W. 2015. An inventory of glacial lakes in the Third Pole region and their changes in response to global warming. *Global and Planetary Change* **131**: 148-157.
<http://dx.doi.org/10.1016/j.gloplacha.2015.05.013>

Table 1. USV specifications

Item	Specification
Dimensions L × W × H	56 × 45 × 16 cm
Weight	5.5 kg
Power	2 × 5800 mAh 11.1V LiPo batteries
Speed	~3 km/h
Sonar	Furuno 235dt-pse 235 kHz Maximum depth reading: 100 m 1 measurement per second Accuracy: ±3%
Assembly time	15 minutes
Remote control range	150 metres

Accepted Article

Table 2. Supraglacial pond characteristics

Pond ID	Area (m ²)	Volume (m ³)	Maximum depth (m)	Connectivity (I – Isolated, C – connected, CI – connected with ice cliff present)	Circularity	Notes
K1	943 ± 36	1443 ± 41	5.5	I	1.90	
K2	2729 ± 63	9049 ± 111	9.9	I	2.37	
K3				C		Data gaps*
K4	958 ± 34	1460 ± 29	3.5	CI	1.83	
K5				CI		Data gaps*
K6	4010 ± 56	19042 ± 119	9.1	I	1.28	
K7	255 ± 10	379 ± 18	4.3	I	1.38	
K8	250 ± 13	445 ± 18	4.4	C	1.14	
K9	5422 ± 54	26959 ± 213	14.6	CI	3.47	
K10	392 ± 11	752 ± 24	4.5	I	1.27	
K11	600 ± 28	882 ± 22	3.4	CI	1.98	
K12	3654 ± 107	5746 ± 158	6	CI	6.63	
K13	231 ± 10	342 ± 13	3.3	I	1.14	
K14	39 ± 6	24 ± 4	1.3	I	1.36	
K15	596 ± 18	1087 ± 28	4	CI	1.73	
K16	625 ± 16	1497 ± 32	5.5	I	1.55	
K18	6482 ± 119	30058 ± 293	13.5	C	3.40	
K19	1193 ± 59	2116 ± 66	6.1	C	4.00	Main drainage event 19-25/07/16
K20	3502 ± 56	13369 ± 163	8.8	CI	2.61	Drainage initiation on 19/07/2016
K21	18744 ± 97	290928 ± 1528	45.6	CI	1.56	
K22	754 ± 24	1634 ± 28	4.5	I	1.27	Drained 27-29/08/16
K23						Drainage initiation on 02/07/16
L1	3789 ± 38	16986 ± 101	9.8	CI	1.63	
L2	207 ± 10	235 ± 16	3.1	C	2.05	
L3	318 ± 11	496 ± 19	4.3	C	1.53	
L4	13101 ± 192	71514 ± 502	17.2	CI	2.71	
L5	1530 ± 40	2789 ± 42	4	C	1.84	

*Bathymetry not used due to partial pond coverage

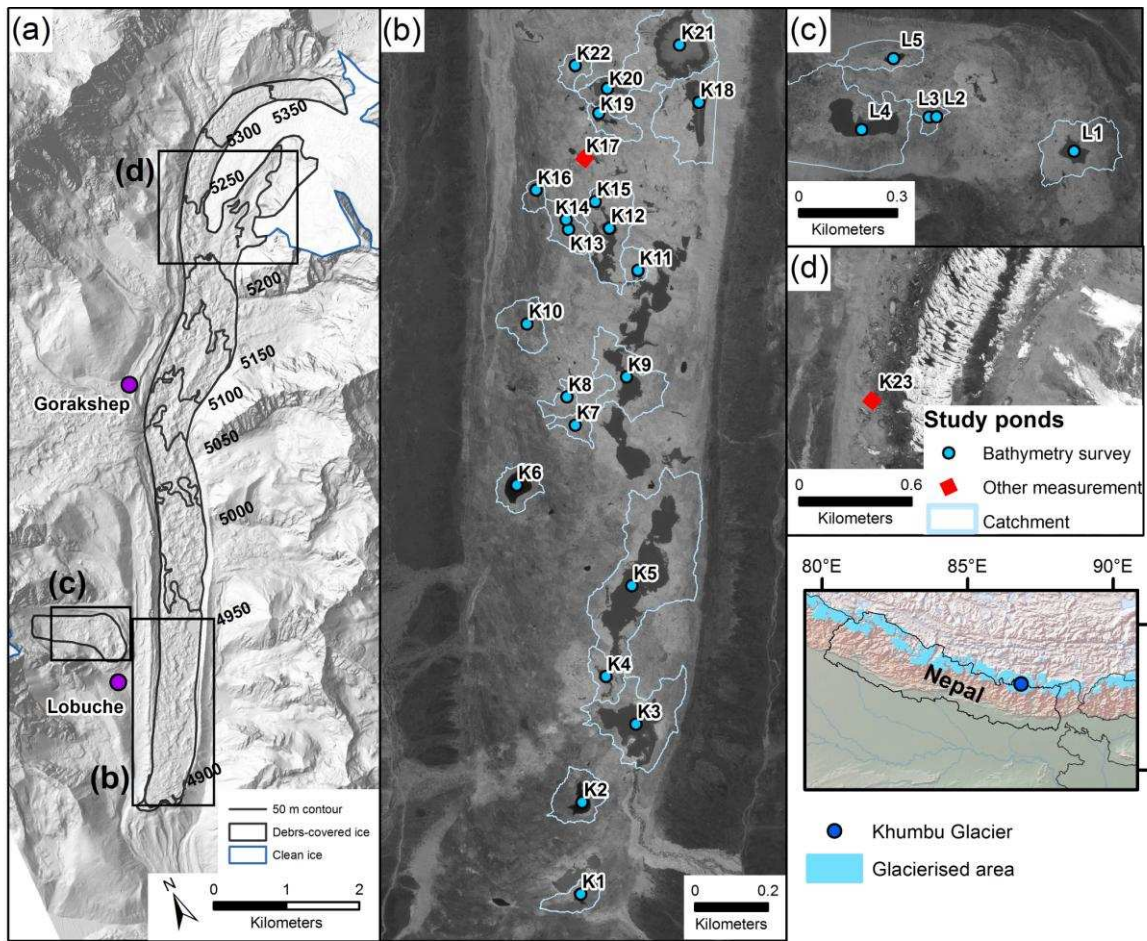


Figure 1. (a) The location of the study ponds on Khumbu and Lobuche Glaciers, Nepal with a hillshaded Pleiades DEM background. (b) The lower terminus of Khumbu Glacier (c) The disconnected terminus of Lobuche Glacier. (d) The upper ablation zone of Khumbu Glacier at the transition from debris-covered to clean ice. Pond catchments are shown as light blue polygons (b and c). Inset backdrops are a panchromatic Pleiades satellite image (16th May 2016).

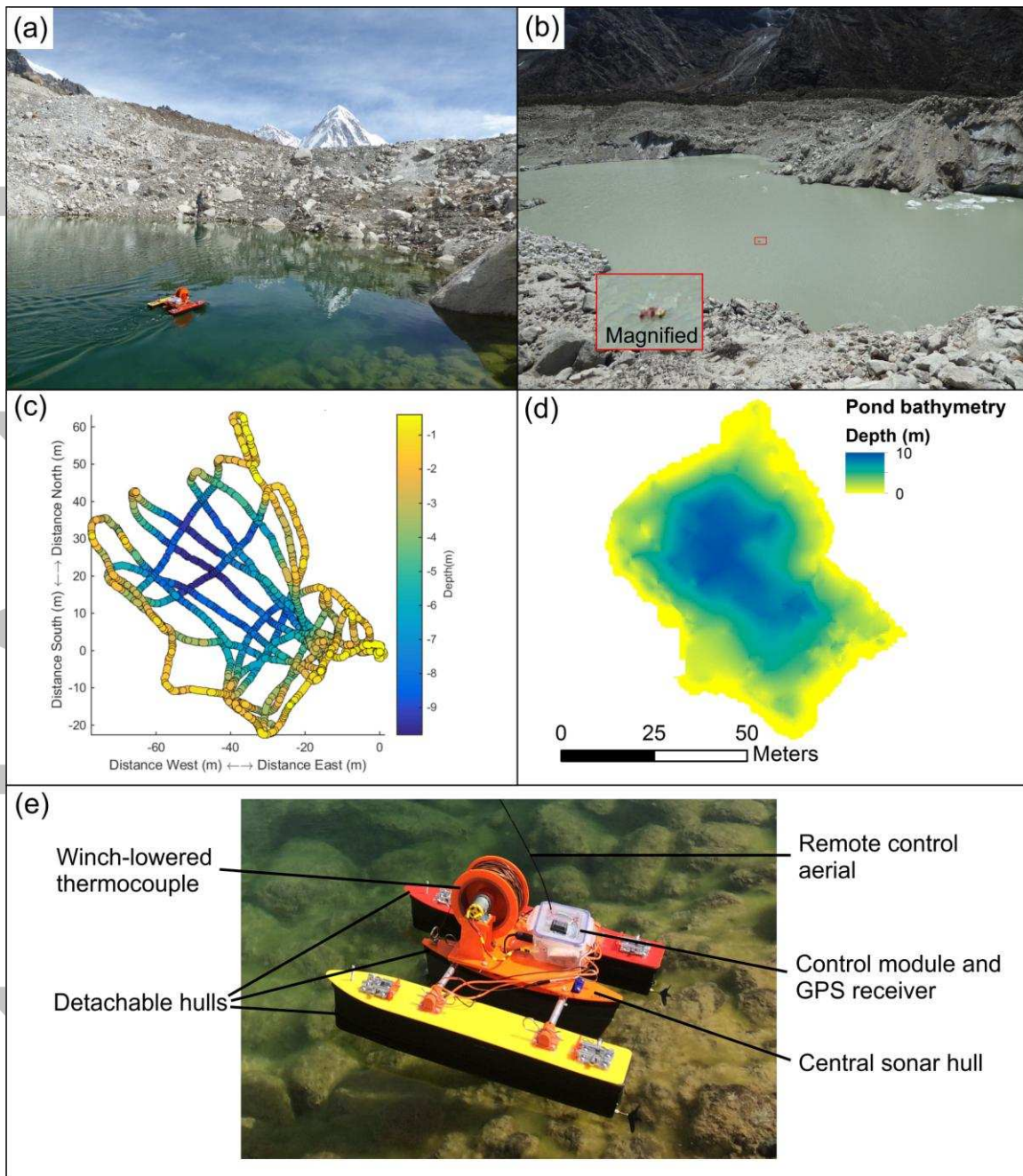


Figure 2. (a) The unmanned surface vessel deployed on a small isolated 'green' pond with no ice cliffs present, and (b) a large connected highly-turbid 'grey' pond with ice cliffs. (c) An example of the point depth measurements collected during a survey, and (d) bathymetry derived by interpolation of the data in (c). (e) The unmanned surface vehicle and modular components.

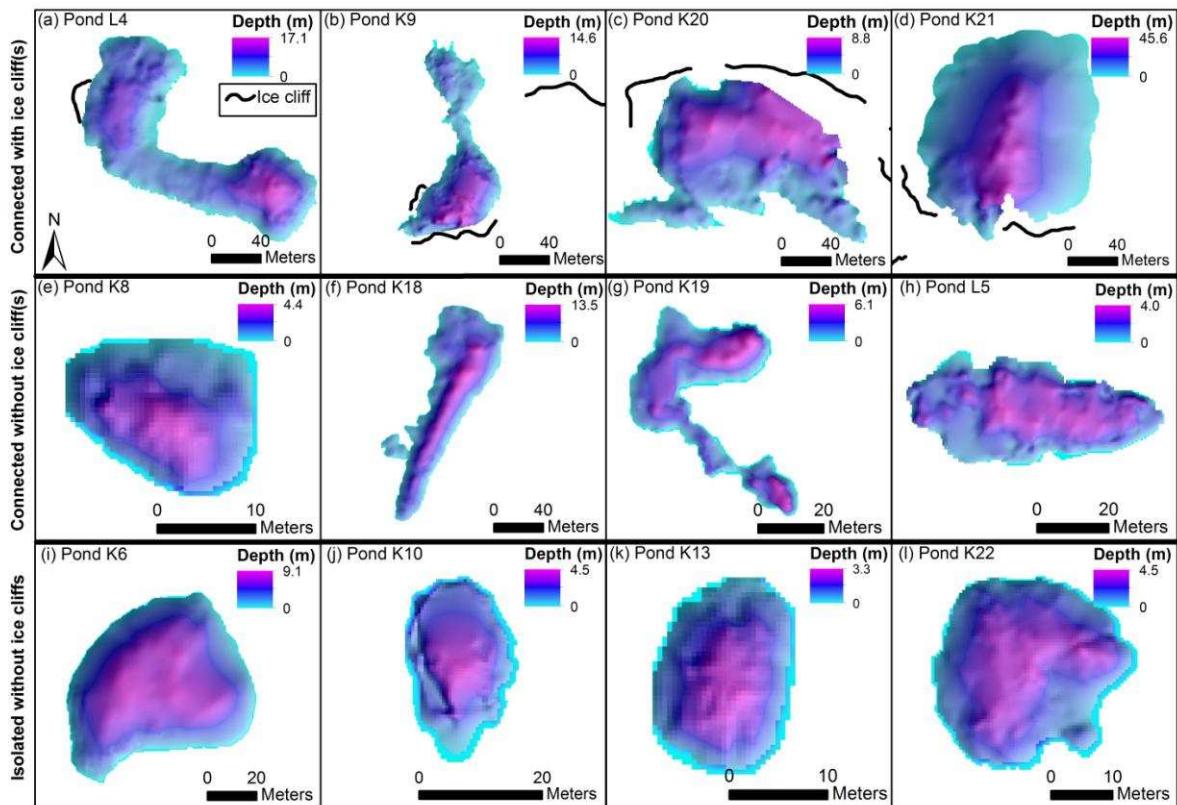


Figure 3. Examples of pond bathymetry for connected ponds with ice cliffs (a–d), connected ponds without ice cliffs (e–h), and isolated ponds (i–l). The top edge of adjacent ice cliffs are shown as black lines. Note different scales between panels. A smoothed (low-pass filter) hillshade overlay is shown with transparency.

Accepted

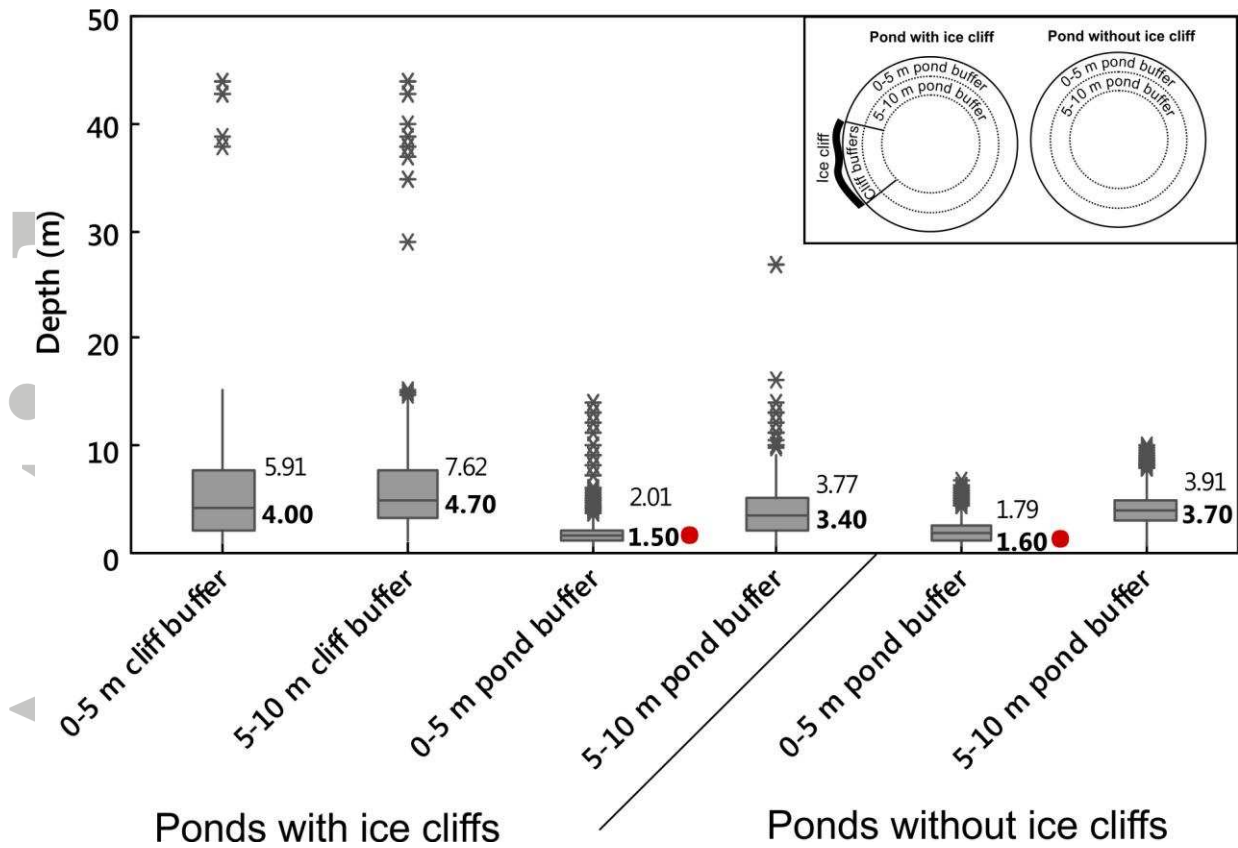


Figure 4. Depth characteristics of all ponds with and without cliffs using the raw data points sampled with buffers (illustrated in the inset). All buffers were tested against each other using pair-wise Mann-Whitney U tests. Medians were statistically significant at $p < 0.05$ unless indicated with a red circle.

Accepted

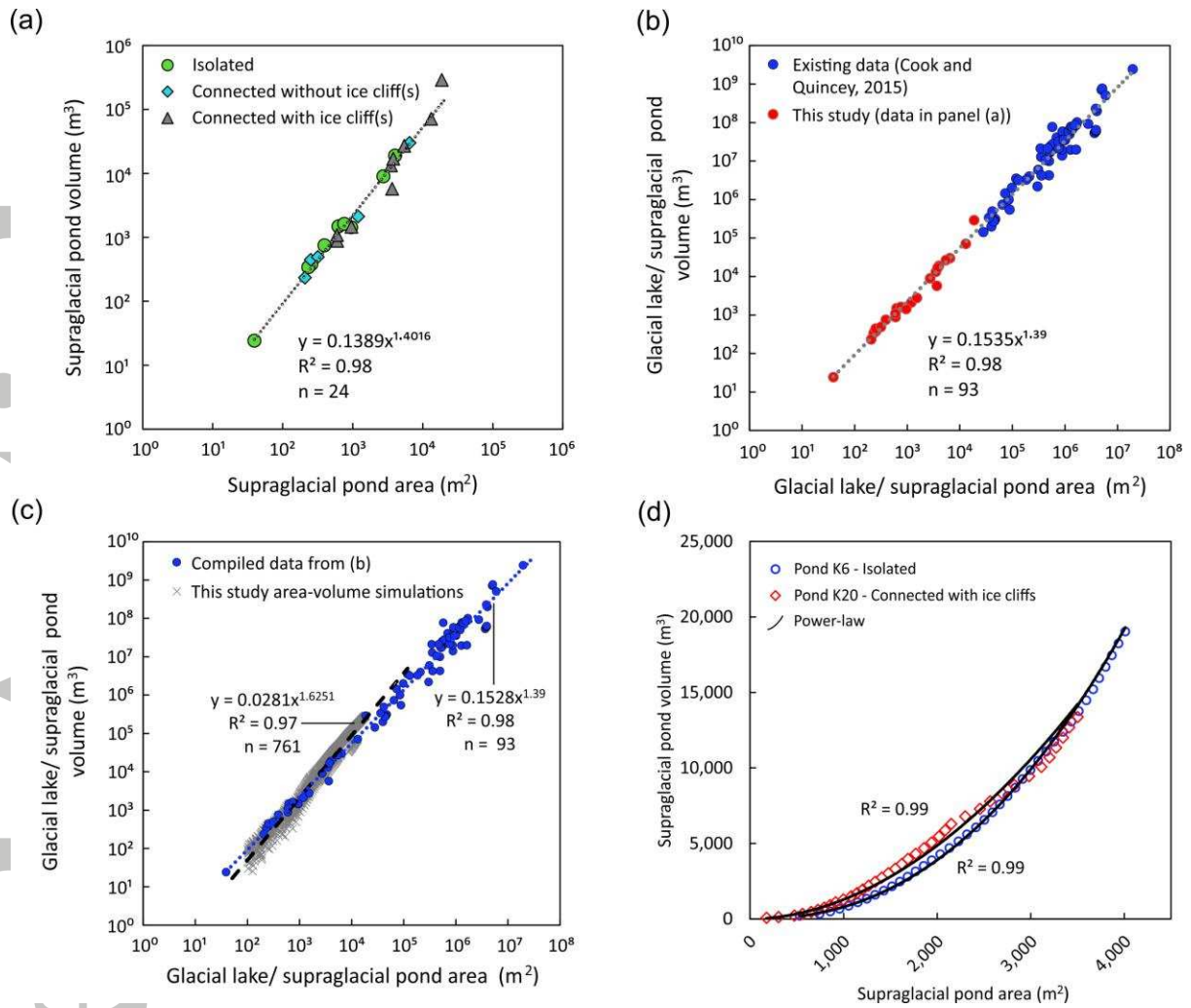


Figure 5. (a) Area-volume relationships derived from data in this study. (b) The data of this study combined with the compiled dataset of Cook and Quincey (2015). (c) The data of (b) with additional datapoints from simulating the drainage of surveyed ponds. (d) The area-volume relationship for ponds K6 and K20 during simulated drainage.

Accepted

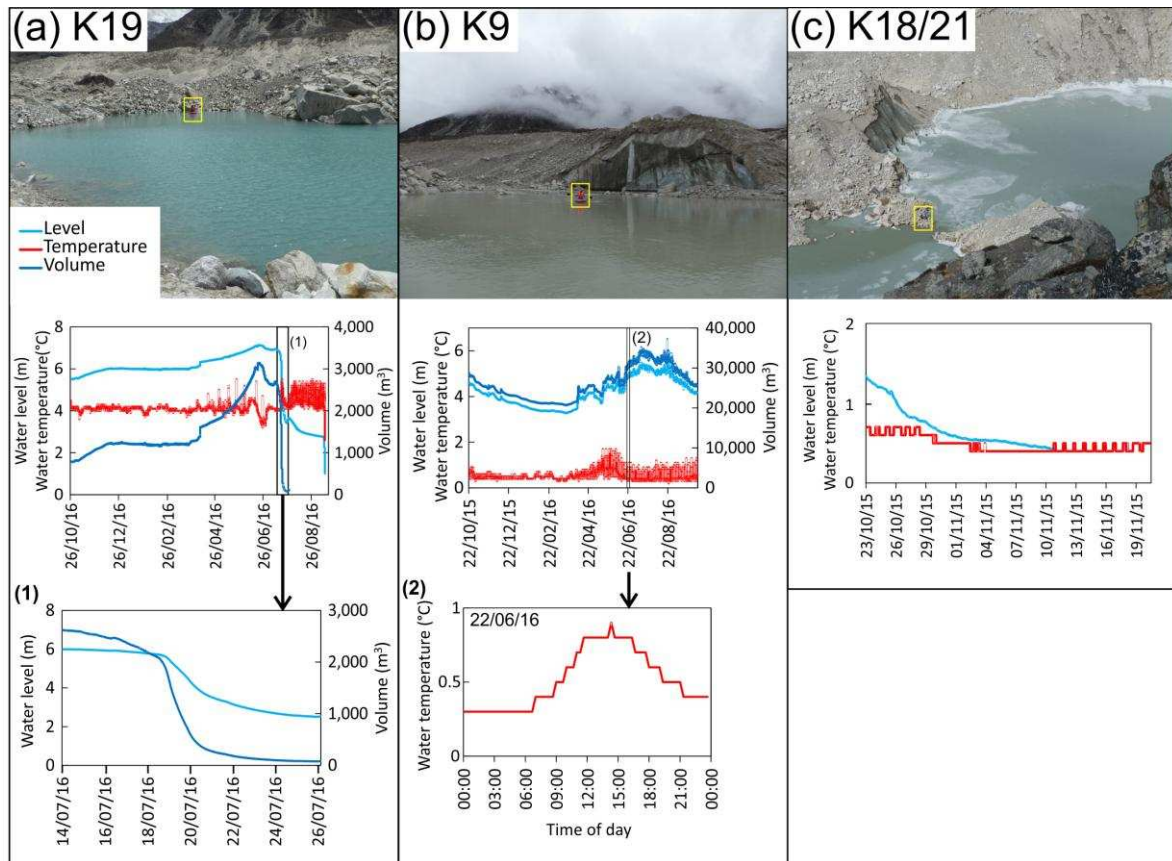


Figure 6. Water level and temperature for (a) K19, (b) K9, and (c) K18/21. Slumped ice plates are visible along the shoreline of K21 in November 2015 (c). Pond bathymetry was used to derive a volumetric time series for (a) and (b). Pond temperatures represent the pond bed. Yellow rectangles indicate the author for scale. Dates are dd/mm/yy.

Accept

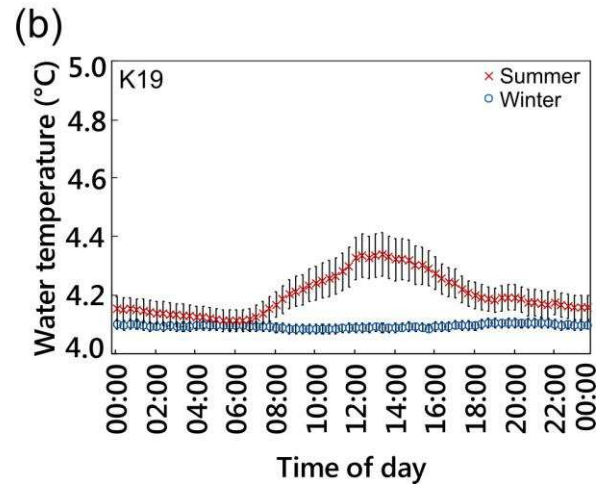
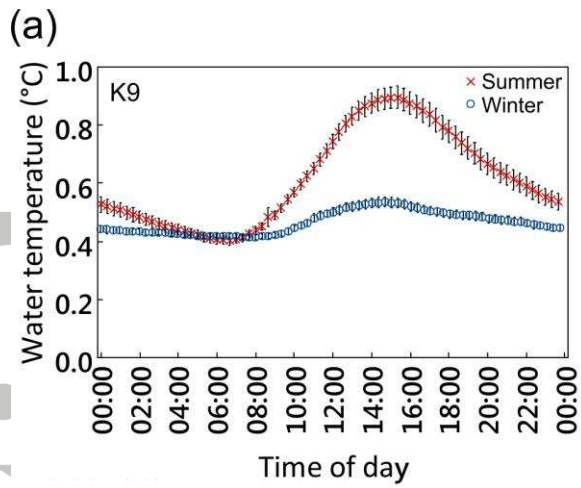


Figure 7. Mean and standard deviation of 20 minute daily pond bottom water temperatures for ponds (a) K9 and (b) K19. Note the broken y-axis (b). Winter and summer intervals are 28/10/15–19/03/16 and 20/03/16–01/09/16 respectively.

Accepted Article

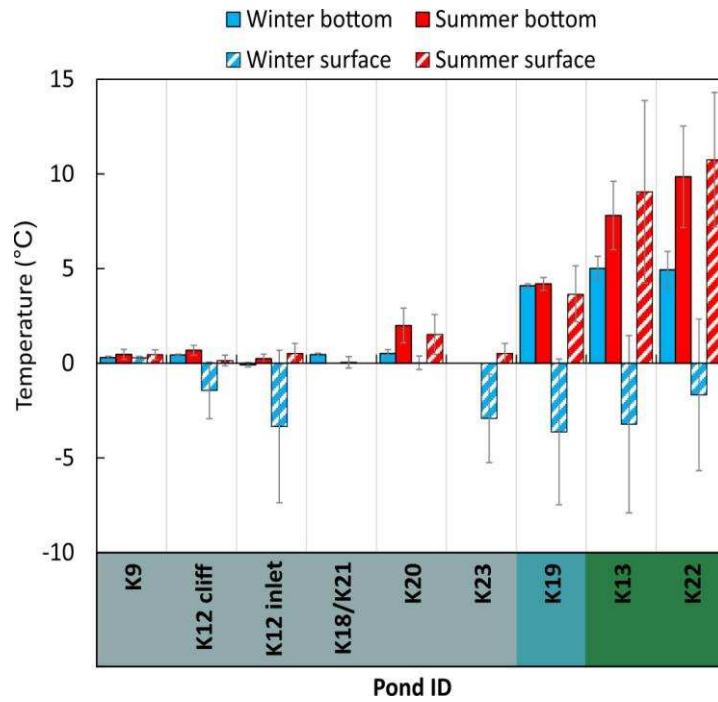


Figure 8. Seasonal supraglacial pond bottom and surface water mean temperatures. Error bars indicate one standard deviation. Coloured x-axis represents indicative pond colour for connected ponds with an ice cliff (grey), connected ponds without an ice cliff (turquoise), and isolated ponds (green).